

Biochemical Characterization of the Interaction between Rab Proteins and Myosin XIa in the  
moss *Physcomitrella patens*

A Major Qualifying Project Report

submitted to the faculty of

Worcester Polytechnic Institute

in partial fulfillment of the requirements for the

Degree of Bachelor of Science

by

Jennifer Mary Garbarino

Sarah Elizabeth Kaptur

Date: 4/30/2015

# TABLE OF CONTENTS

---

Table of Figures .....	iv
Table of Tables .....	iv
Acknowledgements.....	v
Abstract.....	vi
1.0 Introduction and Background .....	1
1.1 Polarized Growth.....	1
1.2 Physcomitrella patens.....	2
1.3 Actin Cytoskeleton.....	3
1.4 Myosin Motors .....	4
1.5 Rab GTPases .....	6
1.6 Known Interactions between Rabs and myosin .....	8
1.6.1 Myo2p and Ypt31/32p in Yeast.....	9
1.6.2 Myo5B and Rab11 in Mammalian Cells .....	10
1.6.3 Other Factors Effecting Myosin-Rab Binding.....	12
1.6.4 Mutagenesis Strategy in Myosin XIa.....	13
1.6.5 Modelling of Myosin XIa GTD .....	14
1.7 Purpose of study.....	15
2.0 Methodology .....	16
2.1 Q5 Mutagenesis.....	16
2.2 Protein Purifications.....	17
2.2.1 Myosin XIa Coiled Coil Tail (CCT) Wild Type and Mutants.....	17
2.2.2 Rab GTPases Wild Type and Mutants.....	19
2.3 Binding Studies .....	20
2.3.1 Twelve Point Binding Curves.....	20
2.3.2 12.5 nM Binding Study Methodology .....	21
2.3.3 2.5 $\mu$ M Binding Study .....	22
3.0 Results.....	23
3.1 Site Directed Mutagenesis.....	23
3.2 Protein Purifications.....	24
3.2.1 Wild type and Mutant Myosin XIa-CCT Purification .....	24

3.2.2	RabA21, A41, and A53 WT and RabA21 Mutants Purification .....	27
3.3	RabA-Myosin XIa-CCT Binding Studies .....	28
3.3.1	Binding Curve .....	28
3.3.2	Binding Differential (12.5 nM).....	29
3.3.3	Binding Differential (2.5 $\mu$ M) .....	31
3.3.4	RabA21 Nucleotide Locking .....	32
4.0	Discussion .....	34
6.0	References.....	38

## TABLE OF FIGURES

---

<b>Figure 1: Model for tip growth in <i>P. patens</i>.</b>	4
<b>Figure 2: Schematic of <i>P. patens</i> myosin XIa</b>	5
<b>Figure 3: Phylogeny of the aligned RabA family from <i>A. thaliana</i> and <i>P. patens</i></b>	8
<b>Figure 4: Structural overview of the Myo2p GTD</b>	9
<b>Figure 5: Crystal structure of Rab11-GTP (grey) bound to Myo5B-GTD (red)</b>	10
<b>Figure 6: Schematic view of the Rab11-GTP-Myo5B interactions</b>	11
<b>Figure 7: Lack of complementation of function using RNAi</b>	13
<b>Figure 8: Pymol modelling of myosin XIa against Myo5B</b>	14
<b>Figure 9: PCR product from Q5 mutagenesis reactions for myosin XIa and RabA21</b>	23
<b>Figure 10: Purification of myosin XIa (MW 58kDa)</b>	25
<b>Figure 11: Myosin XIa ninhydrin assay</b>	26
<b>Figure 12: RabA wild type and mutant purification</b>	27
<b>Figure 13: Twelve point binding curve experiments</b>	28
<b>Figure 14: Binding differentials experiment (12.5 nM)</b>	30
<b>Figure 15: Binding differentials experiment (2.5 <math>\mu</math>M)</b>	31
<b>Figure 16: Binding differentials (2.5 <math>\mu</math>M) RabA21 mutants</b>	33

## TABLE OF TABLES

---

<b><i>Table 1: Primers for Q5 mutagenesis of myosin XIa and RabA21</i></b>	16
<b><i>Table 2: Concentration of myosin XIa and volumes added in 12 point binding studies</i></b>	21

## ACKNOWLEDGEMENTS

---

We would like to thank the following individuals, organizations, and institutions for their guidance and support throughout the course of this project:

- Dr. Mary Munson from the University of Massachusetts Medical School for co-advising the project, providing a laboratory space, and acting as a mentor throughout the year.
- Dr. Luis Vidali from Worcester Polytechnic Institute for co-advising the project and providing guidance, advice, and support throughout the year.
- Michelle Dubuke and Fabienne Furt for their day-to-day technical support in the lab, as well as helpful advice and discussion regarding the project.
- All members of the Munson and Vidali labs for their support and ideas throughout the course of the year which made the project possible.
- Worcester Polytechnic Institute and the University of Massachusetts Medical school for co-sponsoring the project.
- The National Science Foundation and the National Institutes of Health for funding the research.

## ABSTRACT

---

In *Physcomitrella patens*, actin-mediated trafficking and myosin XIa are essential for polarized growth. In other model organisms, the association between myosin and its cargo is mediated by Rab-GTPases. We cloned and purified wild type and mutants of moss myosin XIa that fail to complement an RNAi myosin XIa loss-of-polarity phenotype. Through binding assays, we identified RabA21 as having potential myosin XIa binding activity. The disruption of this interaction may be responsible for the lack of rescue of the phenotype.

# 1.0 INTRODUCTION AND BACKGROUND

---

## 1.1 POLARIZED GROWTH

In the eukaryotic cell, the organization of proteins, membranes, and organelles allows for many complex processes to occur. In fact, directed movement and the resulting organization is essential for life (Wickner, 2008). The processes of cell growth and division, in particular, rely upon the directed movement and organization of various components. When cells grow in a polarized fashion, or in one specific direction rather than uniformly, the need for various materials to be brought to the growing tip of the cell requires subcellular organization.

Many types of cells undergo the process of polarized cell growth and therefore are key systems for understanding the molecular mechanisms by which their respective subcellular organization is accomplished. In mammalian systems, epithelial, neuronal, and many other types of cells undergo polarized growth. For example, epithelial cells grow towards the apical and basal sides of the cell. Neurons extend only at the apex of the cell by using the cytoskeletal matrix and calcium signaling to form synapses. In plants, pollen tube cells and root hairs from vascular plants, and protonemal cells from bryophytes also experience this phenomenon. The ability of these cells to extend extraordinarily in length relative to their width not only requires coordinated growth, but also confers unique function. For example, plant pollen tubes experience extremely rapid polarized growth (250 nm/s in lilies) so that they can search for an ovule, which allows for fertilization and sexual reproduction to occur (Cole and Fowler, 2006). Furthermore, plant root hairs utilize polarized growth (10-40 nm/s) to obtain minerals and water from the soil that are critical for the growth of the plant (Vidali and Hepler, 2001).

The process of polarized growth, and the proteins needed to coordinate the process, are conserved from single celled eukaryotes to the multicellular organisms described previously. For example, budding yeast, the traditional model organism for studying polarized growth, divides when the daughter yeast cell grows and buds off the mother yeast cell at a specific location along the plasma membrane. The coordination of the cytoskeletal network, molecular motors, and effectors allows for the creation of the gradients needed for polarized growth (Pruyne D., 2000). One species that experiences polarized cell growth is *Physcomitrella patens*, a species of moss traditionally used as a model system to study plant evolution and development.

## **1.2 PHYSCOMITRELLA PATENS**

The bryophyte, *Physcomitrella patens*, can also be used as a model system for studying polarized growth, specifically tip growth. The tissues in the moss, *P. patens*, which grow in a polarized fashion are protonemata, including chloronemata and caulonemata (Menand et al., 2007). Chloronemata are the most basic cell type in *P. patens* and are characterized by a perpendicular cell wall and a large number of chloroplasts. Chloronemata grow at a rate of 1.5 nm/s and divide approximately every 24 hours (Vidali and Bezanilla, 2012). By contrast, caulonemal cells have oblique cell walls and fewer chloroplasts. Caulonemata grow at a rate of 5-10 nm/s and divide every 7 hours. Growing caulonemal cells also have tips that are lacking large organelles, but are instead filled with material needed for cell wall deposition and cell growth (Cove and Knight, 1993). Materials for polarized tip growth are transported through the cell's cytoskeleton network through trafficking along actin. *P. patens* is a useful model system due to its ability to be genetically modified, and its pluripotency (Vidali and Bezanilla, 2012). Genetic modifications occur using homologous recombination, which in *P. patens* can happen with up to 100% frequency, whereas in flowering plants, it occurs at a rate of  $10^{-4}$ - $10^{-5}$  (Kamisugi

et al., 2006). This makes *P. patens* ideal for knock-outs, knock-ins, and RNA interference (RNAi) strategies (Kamisugi et al., 2006). The genome of *P. patens* has been sequenced, which makes genetic manipulations easier as well (Rensing et al., 2008). *Physcomitrella patens* is also ideal for microscopy because of the large cell size and organization into a monolayer.

### 1.3 ACTIN CYTOSKELETON

Many eukaryotic cells, including the protonemata of *P. patens*, use cytoskeletal networks to orchestrate subcellular polarization. Cytoskeletal networks in plants cells, including those of *P. patens*, are composed of microtubules and actin filaments. Discovered in muscle tissues in the 1940s, cellular concentrations of actin make it one of the most ubiquitous and abundant proteins (Pollard T.D., 2009).

In many types of cells, actin monomers polymerize into long, stable filaments that act as subcellular pathways for the trafficking of proteins. Actin filaments grow in a polarized fashion by adding ATP-actin monomers on one end (barbed end), hydrolyzing the gamma phosphate, and leading to the dissociation of the ADP-actin monomer on the opposite end (pointed end). Over 100 accessory proteins control the polymerization of actin, including regulating elements such as the length, the turnover, and branching of actin filaments (Pollard T.D., 2009). One class of proteins that utilize the actin cytoskeletal network are myosin motors, which interact with actin to create the mechanical force necessary to transport various cargos throughout the cell.

In *P. patens*, the material transported along the actin cytoskeleton is hypothesized to be necessary for polarized cell growth to the tip of the cell. **Figure 1** shows a model illustrating the cell machinery thought to be used in this process.

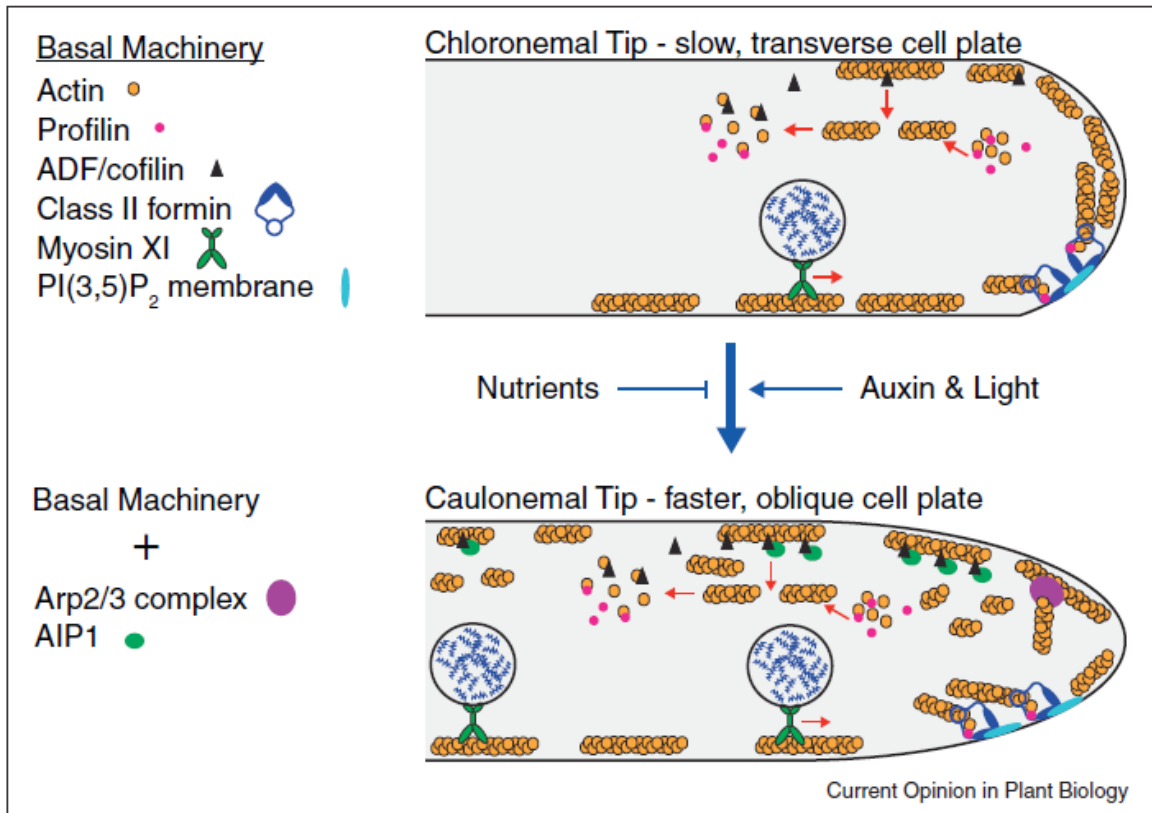


**Figure 1: Model for tip growth in *P. patens* (Vidali and Bezanilla, 2012).**

In this model, actin is polymerizing and depolymerizing near the cell membrane. This process is regulated by the basal machinery of profilin, actin depolymerizing factor, and class II formin, which binds to PI(3,5)P<sub>2</sub>. The motor protein myosin XIa is then able to move down the existing actin filament, carrying the cargo needed to continue growth (Vidali and Bezanilla, 2012).

## 1.4 MYOSIN MOTORS

Myosins belongs to a family of motor proteins that are involved in many different cellular processes including organelle trafficking, cytokinesis, maintenance of cell shape, muscle contraction, and polarized growth (Scholey J. M., 2003; Vale, 2003; Yumura S., 2003; Geeves, 2005; Vidali et al., 2010). Phylogenetic analysis of myosins reveals 35 classes, making them one

of the most prevalent and divergent families of proteins (Bernardo J. Foth, 2006; Maravillas-Montero J., 2012). Most myosins utilize actin filaments by using the energy of ATP hydrolysis to “walk” towards the barbed end of the filament with defined step sizes that vary between myosin classes.

In *P. patens*, the functionally redundant proteins myosin XIa and myosin XIab are the homologues of animal and yeast class V myosin. These proteins are hypothesized to function as processive molecular motors carrying various cargoes along actin filaments and organizing cells. The protein, which has a molecular weight of 174.34 kDa, dimerizes and consists of four domains is shown in **Figure 2** (Vidali et al., 2010).

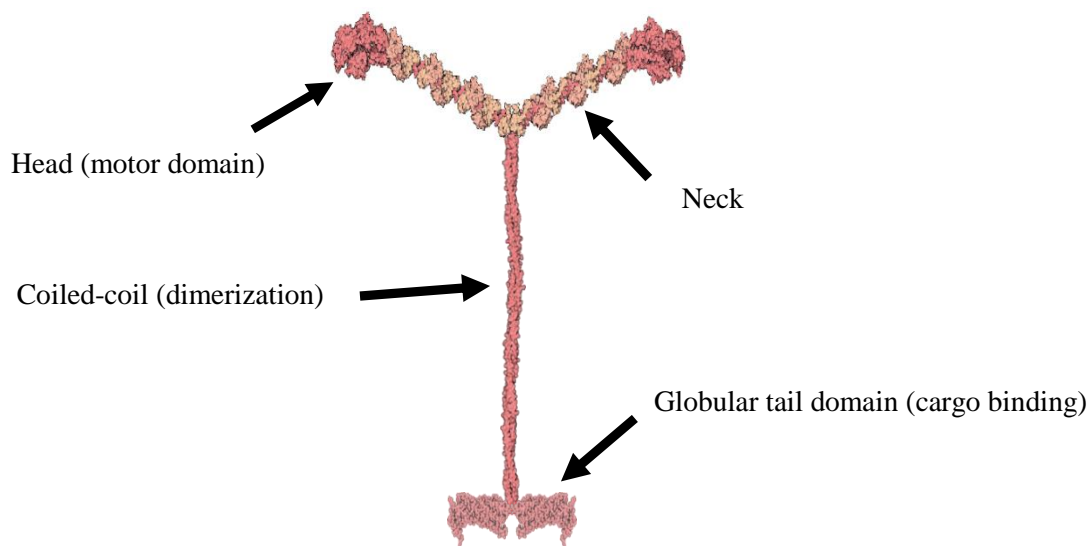


**Figure 2: Schematic of *P. patens* myosin XIa** [Adapted from (Goodsell, 2001)]

The head domains, also termed the motor domains, bind to actin filaments to generate the mechanical force of the motor via the hydrolysis of ATP. Two head domains are attached to two neck domains, which consist of six IQ calmodulin binding motifs each. The neck domains connect to the coiled-coil domain, which is required for the dimerization of myosin XIa *in vivo*. The final domain on the C terminus is the globular tail domain (GTD), also called the cargo

binding domain (CBD). This domain allows class V myosins to specifically bind various cargoes, including secretory vesicles. The cargo binding domain as well as a small portion of the coiled-coil domain (64 amino acids) is soluble and can be purified (Jacques, 2013).

In *P. patens*, there are two functionally redundant isoforms of myosin XIa: myosin XIa and myosin XIab. In the caulonemal and chloronemal cells of *P. patens*, myosin XIa is necessary for normal polarized growth, as a knockdown of both isoforms of myosin XIa inhibits polarized growth. In protonemal cells, myosin XIa travels along actin filaments, localizing to the growing tip of the cell (Vidali et al., 2010).

The GTD of class V myosins plays a role in selective cargo recruitment of the molecular motor and the regulation of motor activity. The GTD is also known to interact both directly and indirectly with various other proteins, including Rab GTPases. The GTD itself contains two subdomains which have been shown in mammalian Myo5B, the homologue of myosin XIa, to allow for the selective binding of different cargoes (Pashkova et al., 2005; Pylypenko, 2013).

## **1.5 RAB GTPASES**

Many proteins are necessary for regulating membrane traffic. The Rab family of small GTPases typically activate the transport of vesicles and the recognition, tethering, and fusion of vesicles to their target compartment. Rab proteins are molecular switches which are prenylated on their C-terminal domain to insert into the target membrane. These proteins are activated and deactivated by their nucleotide state, which is controlled by additional proteins: guanine nucleotide exchange factors (GEFs) that replace GDP with GTP to activate them, and GTPase-activating proteins (GAPs) that activate the Rab's hydrolysis of GTP to GDP, to deactivate them. Additionally, Rab GDP dissociation inhibitors (Rab GDI) bind to a Rab in the GDP form and

prevent the dissociation of GDP. This allows the Rab to be reactivated off the membrane by the GEF and re-bound to a new target membrane (Mizuno-Yamasaki, 2012). The GEF is also used to target Rab proteins to the membrane. It is hypothesized that the Rab binds non-specifically to the membrane multiple times until it meets the proper GEF that allows it to remain on the membrane for a longer period (Barr, 2012). Rab proteins tend to be activated in their GTP bound state. This has been seen in a yeast Rab5/Vps21p tethering study where the interaction required the GTP-loaded form (Lo et. al 2012). However, in a further study of human Rab proteins, three Rab proteins (Rab2a, Rab5a and Rab7a) were found to have activity (measured through liposome aggregation) without any nucleotide and adding GTP or GDP did not significantly change this activity (Tamura, 2014).

Rab proteins are very ubiquitous, with over 8,000 Rab proteins occurring in 247 different genomes. There are 44 subfamilies in humans, 55 in *P. patens*, and 11 in yeast (Ciencia, 2011). The RabA family in moss is hypothesized to bind to myosin XIa due to its homology to the mammalian Rab in this interaction. The RabA phylogeny tree is shown in **Figure 3** (Agar, 2013).

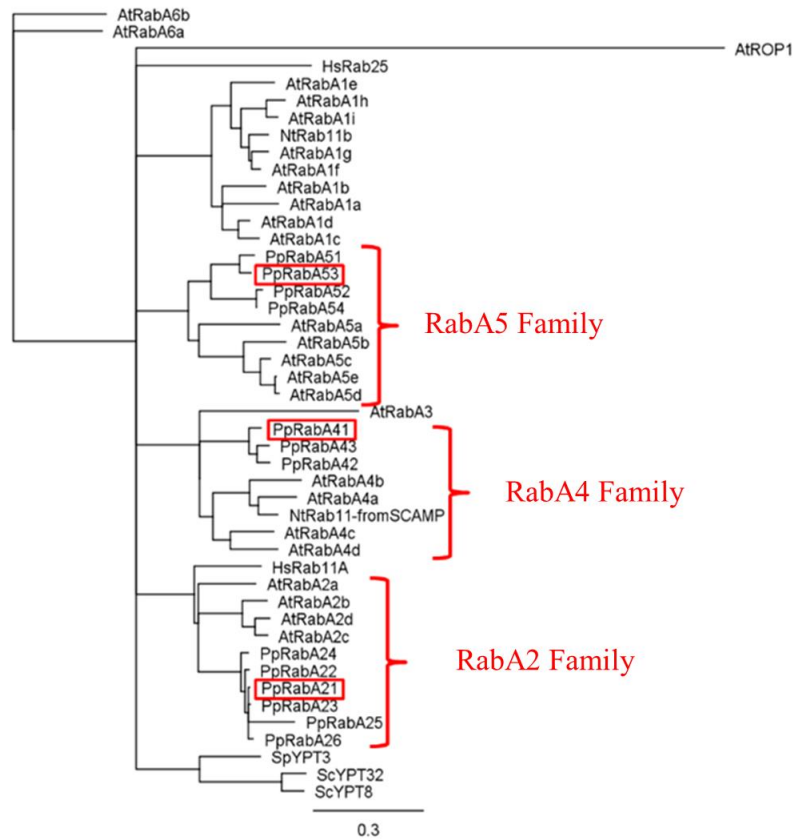


**Figure 3: Phylogeny of the aligned RabA family from *A. thaliana* and *P. patens***  
 Representative *P. patens* Rab proteins used in this project are boxed in red (Agar, 2013)

Representative Rabs from three of the RabA subfamilies (RabA2, RabA4, RabA5) were chosen for future analysis. Previous studies show each of the Rabs highlighted localizes to the tip of a moss cell, and so are potential candidates for binding to myosin XIa (Callahan, 2014).

## 1.6 KNOWN INTERACTIONS BETWEEN RABS AND MYOSIN

The interactions between Rab GTPases and class V myosins have been previously studied using both *S. cerevisiae* and mammalian cells. The yeast and mammalian homologues, Myo2p and myosin V respectively, have both been crystallized, suggesting a putative binding region for Ypt31/32p or Rab11 respectively (Pashkova et al., 2006; Pylypenko, 2013). It is

hypothesized that the *P. patens* protein myosin XIa GTD analogously interacts with a RabA to facilitate polarized growth *in vivo*.

### 1.6.1 Myo2p and Ypt31/32p in Yeast

In 2006 the crystal structure of the globular tail domain of the yeast protein, Myo2p, was determined by the Weisman lab; this was the first structure of a class V myosin GTD to be published (Pashkova et al., 2006). The yeast Myo2p GTD was found to consist of 15 alpha helices that form two densely packed subdomains as shown in **Figure 4**. This study also revealed highly conserved regions on opposite surfaces of the GTD that, when mutated, specifically disrupted either secretory vesicle inheritance or vacuole inheritance.

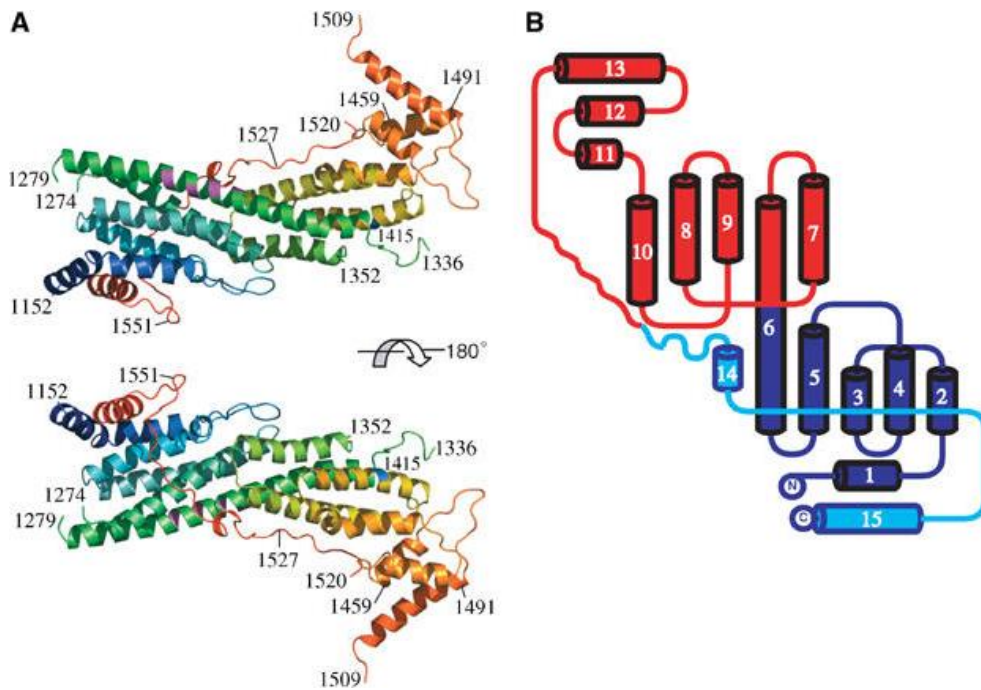


**Figure 4: Structural overview of the Myo2p GTD** A) Ribbon representation of crystal structural from two orientations B) Topology diagram of two subdomains (Subdomain I is blue and Subdomain II is red) (Pashkova et al., 2006)

In a later publication, researchers found that the five mutations that created a deficiency in secretory vesicle inheritance did so by disrupting the binding site of either Ypt31 or Ypt32, the Rab11 homologues in yeast. Furthermore, the direct interaction of GTP-Ypt31/32p and Myo2-GTD is essential for the polarization of Myo2p to sites of cell growth and cell viability. The specific interaction between Ypt31/32p and the Myo2-GTD was identified using a yeast two hybrid screen, and the nucleotide state was confirmed using Ypt31/32p mutants that were constitutively active or dominant negative (Lipatova et al., 2008).

### 1.6.2 Myo5B and Rab11 in Mammalian Cells

The homologous interaction between a mammalian motor (Myo5B) and a Rab GTPase (Rab11) was also recently studied. In 2013, researchers solved the crystal structures of the Myo5B GTD, as well as Myo5B-GTD in complex with both activated and inactivated Rab11 (Pylypenko, 2013). The Myo5B-GTD in complex with Rab11-GTP is shown in **Figure 5**.

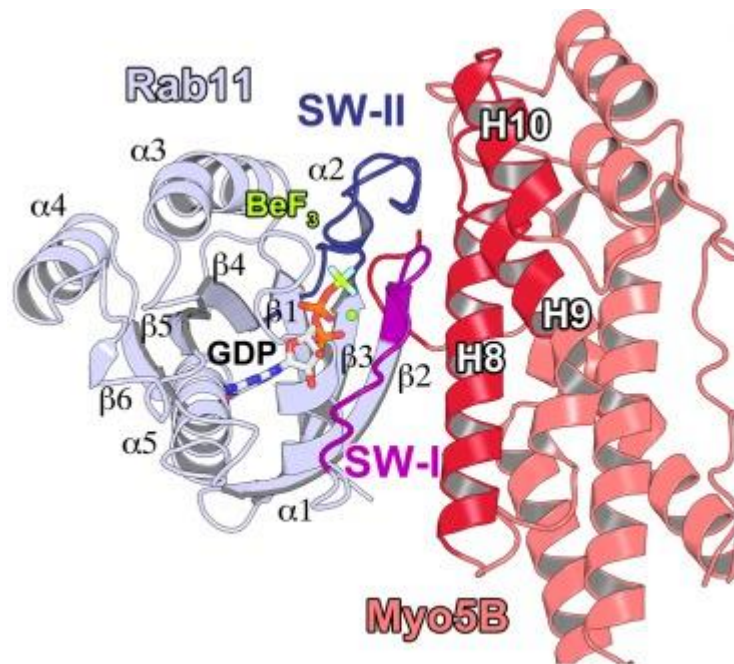


**Figure 5:** Crystal structure of Rab11-GTP (grey) bound to Myo5B-GTD (red) (Pylypenko, 2013)

As seen in **Figure 5**, Myo5B binds Rab11 on the side of subdomain II, composed primarily of Helix 8 as well as portions of Helices 9 and 10 and the loop connecting H5 and H6. By comparing crystal structures of the activated and inactivated forms of Rab11, researchers showed that Rab11, in its active GTP-loaded form, binds to the GTD inducing a dramatic conformational change. This change blocks the hydrolysis of the gamma phosphate of the nucleotide, promoting a stable and direct interaction between the Rab and the motor.

As in the yeast studies, several residues on the Myo5B GTD were identified as necessary for Rab11-GTP binding. Several residues were conserved between the yeast and mammalian systems. The residues which disrupted binding are summarized in **Figure 6**.

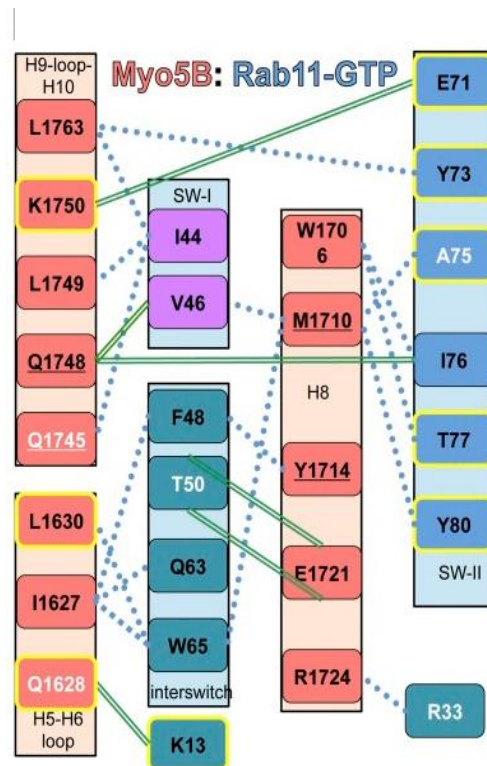


**Figure 6: Schematic view of the Rab11-GTP-Myo5B interactions** (Pylypenko, 2013)

Mutations in the underlined residues result in Rab binding deficiency. Residues conserved between yeast *Myo2p* and vertebrate *Myo5B*, as well as residues conserved within Rabs, are labeled in black. Hydrophobic contacts are shown as dashed lines, hydrogen bonds as double lines. The residues that do not form interactions in the Rab11-GDP to Myo5B interface are highlighted in yellow.

These high resolution crystal structures and the data regarding conserved binding residues served as the basis for the mutant analysis of myosin XIa.

### **1.6.3 Other Factors Effecting Myosin-Rab Binding**

Several other components, including adaptor proteins and vesicle lipid composition have been found to affect interactions between myosin motors and Rab GTPases. For example, several adaptor proteins have been identified as interacting with Rab11. In 2002, a group of *Drosophila* researchers showed that the Rab11-myosin V interaction is mediated by a protein called dRip11 (*Drosophila* Rab11 interacting protein). dRip11 participates in rhodopsin transport in developing photoreceptors through a direct and stabilizing interaction between both Rab11 and myosin V (Li, 2007). FIP2 has also been identified as a Rab11 adaptor in endosome recycling (Cullis, 2002).

In addition to adaptor proteins, the lipid composition of vesicles has also been shown to affect Rab-Myosin interactions. For example, in budding yeast, phosphatidylinositol-4-phosphate (PI4P) is important for the Myo2p dependent trafficking of secretory compartments. In a 2011 study, researchers showed the PI4P was not only present in late secretory compartments, but also critical for the association of the secretory compartments with Myo2p. In fact, enhancement of the interaction of PI4P and Myo2p removed the need for any interaction with the GTPases Ypt31/32p and Sec4p for proper secretory compartment transport. The interaction between PI4P was itself mediated by an unknown adaptor protein (Santiago-Tirado et al., 2011).

### 1.6.4 Mutagenesis Strategy in Myosin XIa

In a previous study in the Vidali lab, nine potential binding sites of the Rab11 homolog were identified on the myosin XIa surface through a comparison to a model based on Myo2p from yeast. The hydrophobic residues that were spatially similar to the Myo2p disruption-of-binding residues were changed to arginines to disrupt binding. These mutants were then screened through a mutant complementation assay (Armstrong, 2012). Myosin XIa and b were knocked down in *P. patens*, by targeting the UTR regions. This causes small round plants with disrupted polarized growth (**Figure 7**, top middle panel). This phenotype can be rescued with the addition of a plasmid containing the wild type gene (without the UTR) (**Figure 7**). Plasmids expressing mutant myosin XIa proteins were tested to determine which mutants, if any, rescued the myosin XIa knockdown phenotype. After seven days of growth the plants were imaged and compared.

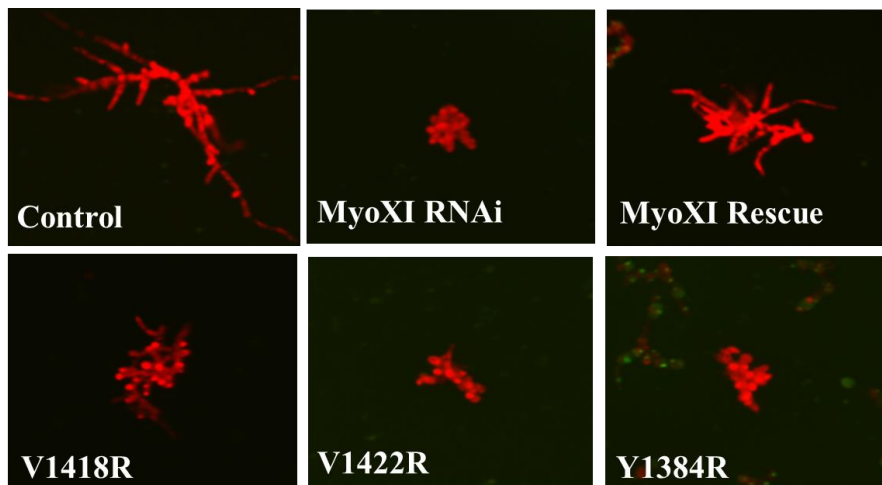
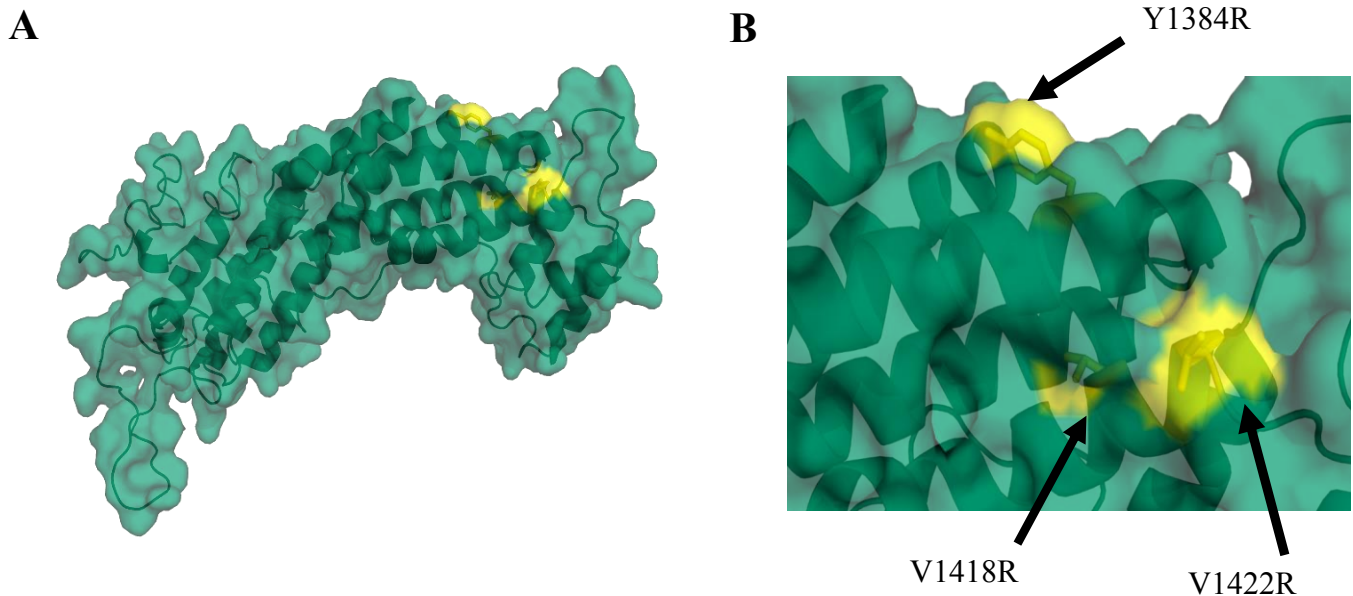


*Figure 7: Lack of complementation of function using RNAi (Armstrong, 2012)*

The three most severe phenotypes are shown in **Figure 7** and were chosen for in-depth biochemical analysis. It is thought that the failure of these mutations to complement the loss of the wild-type protein are due to a disruption of the RabA-myosin XIa interaction.

### 1.6.5 Modelling of Myosin XIa GTD

The Myo5B GTD in complex with GTP-Rab11 crystal structure was published in 2013, providing more insight into the possible structure of myosin XIa when bound to a Rab (Pylypenko, 2013). Recent work in the lab (M. Dubuke, unpublished) used this new structure to update the model of the myosin XIa GTD, which was previously based upon the Myo2p structure (Pashkova et al., 2006). **Figure 8** displays a structural alignment based on sequence homology of myosin XIa GTD to Myo5B GTD.



Unlike Myo2p, the structure of Myo5B GTD was determined in complex with the Rab which allowed the modelling to make more accurate hypotheses about the structure of the myosin XIa globular tail domain when bound to Rab. This updated model, therefore, allowed the various residues on myosin XIa to be much more accurately located on the homology surface. The mutations previously identified and tested in the RNAi complementation assay (Armstrong 2012) were mapped onto the surface of the Myo5B homology model, increasing the accuracy of

their projected placement and orientation. Based on this model, residues 1384 and 1422 were predicted to be surface residues much like with the Myo2p modeling. Residue 1418, however, was predicted to be an internal hydrophobic residue.

## **1.7 PURPOSE OF STUDY**

Polarized tip growth is an important process in many organisms. In *Physcomitrella patens*, myosin XIa trafficking along actin is necessary for polarized growth (Vidali et al., 2010) and myosin XIa association with vesicles may have a regulatory effect on F-actin (Furt et al., 2013). In many other model systems, including yeast and mammalian systems, Rabs are needed to recruit specific cargo to the myosin cargo binding domain (Lipatova et al., 2008; Pylypenko, 2013). It is therefore predicted that a Rab is necessary for recruitment of cargo to myosin XIa in *P. patens*. Based on homology to the mammalian Rab11, it is hypothesized that a RabA is binding myosin XIa to transport cargo needed for polarized growth. In previous studies, mutant myosin XIa proteins were determined to inhibit polarized growth through an RNAi complementation assay, and were predicted to disrupt myosin XIa RabA binding (Armstrong, 2012). This study investigates which RabA binds to myosin XIa and if that binding is disrupted by the myosin XIa mutants from the RNAi complementation assay.

## 2.0 METHODOLOGY

---

### 2.1 Q5 MUTAGENESIS

Mutagenesis for the three selected myosin XIa mutants and three selected RabA21 mutants was completed using the Q5 Mutagenesis Kit from New England Biolabs according to the company protocol (Catalog #: E0554S) The primers used are displayed in Table 1.

*Table 1: Primers for Q5 mutagenesis of myosin XIa and RabA21*

	Forward Primer		Reverse Primer	
Myosin XIa Mutation	ID Number	Sequence	ID Number	Sequence
V1418R	WPI 157	TATATCCGACAAGCACG TGGATTTTTGGTCATTC ATC	WPI 147	CTTGAGCTCATCCCATG ACGCTCCAGCATACTC
V1422R	WPI 146	GCAGTTGGATTTTTGCG CATTCAAAAAGCCA	WPI 150	TTGTCGGATATACTTGA GCTCATCCCATGACGCT CC
Y1384R	WPI 154	TTTAGCAACGGAGAGCG TGTGAAAGCTGGACTT	WPI 158	TGAGCAAACTCACGTC TCAGCAGCAAAGTGT
Rab A21 Mutation	ID Number	Sequence	ID Number	Sequence
S26N	WPI 305	CCGGTGTGGGGAAGAA CAATCTGCTTTCCA	WPI 306	AATCTCCTATCAGCACC ACCTTGAACAG
Q71L	WPI 307	GGGACACAGCAGGGCT AGAGAGGTACCGAG	WPI 308	AAATCTGAGCCTTGATC GTCTTTCCATCGAC
N125I	WPI 309	CATGCTGGTGGGGATCA AGTCGGACCTGAA	WPI 310	ATCACAATGTTTCGAGTC CGCGTGGTCTC

12.5  $\mu\text{L}$  of the Q5 master mix (Q5 Polymerase, Q5 Buffer, dNTPs), 10  $\mu\text{M}$  of each primer, 1 ng of template DNA, and 9  $\mu\text{L}$  of autoclaved  $\text{H}_2\text{O}$  were combined in a thin walled PCR tube. The PCR was run for 25 cycles according to the Q5 protocol with an annealing temperature of  $72^\circ\text{C}$  and an extension time of 4 minutes. After the PCR, the presence of DNA was confirmed by running the sample on a 0.7% (w/v) agarose gel. 1  $\mu\text{L}$  of PCR product was then added to 5  $\mu\text{L}$  of KLD reaction buffer, 1  $\mu\text{L}$  of KLD Enzyme Mix, and 3  $\mu\text{L}$  of autoclaved  $\text{H}_2\text{O}$  for ligation. 5  $\mu\text{L}$  of the product was then transformed into 50  $\mu\text{L}$  of New England Biolabs 5 $\alpha$  *E. coli* competent cells (Catalog #: C2987I) and plated on LB-carbenicillin (0.1 mg/ mL) selection plates.

Colonies for each mutation were moved to a 3 mL liquid culture and grown overnight at  $37^\circ\text{C}$ . Then, each culture was mini-prepped with a Qiagen kit (Catalog #: 27104). DNA samples were sent for sequencing to ensure the presence of the desired mutation and to check the fidelity of the Q5 polymerase.

## **2.2 PROTEIN PURIFICATIONS**

### **2.2.1 Myosin XIa Coiled Coil Tail (CCT) Wild Type and Mutants**

BL21(DE3) or BL21(DE3) Codon+ RIL *E. coli* competent cells were transformed with 2  $\mu\text{L}$  of wild-type or mutant myosin plasmid (50-200 ng/ $\mu\text{L}$ ), plated on LB plates with 0.1 mg/ml carbenicillin, and grown overnight at  $37^\circ\text{C}$ . The subsequent colonies were added to a 50 mL starter culture of LB with 0.1 mg/mL ampicillin at  $37^\circ\text{C}$ , grown to an  $\text{OD}_{600}$  of about 1.0 and then split into the desired final culture volume (5-10 L) of LB with 0.1 mg/mL ampicillin at  $37^\circ\text{C}$ . When the  $\text{OD}_{600}$  was between 0.4 and 0.6, the cells were shifted to  $15^\circ\text{C}$  and induced with 0.1 mM IPTG at an  $\text{OD}_{600}$  between 0.6-0.8. The cells were then grown overnight at  $15^\circ\text{C}$ .

After overnight growth, cells were harvested through centrifugation at 4°C at 5000 rpm for 10 minutes in a Sorvall Evolution centrifuge with a SLC-6000 rotor. The supernatant was removed and the pellet was resuspended in 150ml of cold lysis buffer (50 mM NaH<sub>2</sub>PO<sub>4</sub> pH 8.0, 300 mM NaCl, 10mM imidazole, 10% (v/v) glycerol, fresh 5mM β-mercaptoethanol, 1mM PMSF, DNase, and 1 Protease Inhibitor Tablet (Roche Diagnostics) added prior to lysis). Then cells were lysed using a microfluizer cell disrupter (Microfluidics) at 80 psi. Lysed cells were centrifuged at 13000 rpm in a Sorvall SS-34 rotor for 30 minutes at 4°C.

The supernatant was added to 10 mL of Ni-NTA agarose bead slurry (Qiagen) pre-equilibrated in cold lysis buffer. The slurry then rocked on a nutator at 4°C for 60 minutes, and the bound beads were added to an empty gravity flow column at 4°C. The column was washed with 50 mL of cold wash buffer (50 mM NaH<sub>2</sub>PO<sub>4</sub> pH8.0, 300 mM NaCl, 20 mM imidazole, 10% (v/v) glycerol, fresh 5 mM β-mercaptoethanol added prior to washing). The protein was eluted off the beads into 1 mL fractions by filling the column with cold elution buffer (50 mM NaH<sub>2</sub>PO<sub>4</sub>, 300 mM NaCl, 250 mM imidazole, 10% (v/v) glycerol; pH8.0, fresh 5 mM β-mercaptoethanol added prior to elution). Fractions containing proteins were determined through spotting 5 µl of each fraction onto Wattman paper and staining with Coomassie Blue. Protein-containing fractions were pooled together and diluted to a 100 mM NaCl concentration in MonoQ Buffer A (10 mM Hepes pH 7.5, 10% (v/v) glycerol, 1 mM DTT).

The protein was then loaded onto a MonoQ 10/10 column (GE LifeSciences) pre-equilibrated in Buffer A (see above) with 10% (v/v) Buffer B (10 mM Hepes pH 7.5, 1 M NaCl, 10% (v/v) glycerol, 1 mM DTT). The column was eluted over a gradient of 10%-50% Buffer B over 20 column volumes with 2 mL fractions taken throughout. A 12% SDS-PAGE gel was run with aliquots of fractions corresponding to A<sub>280</sub> chromatograph peaks and stained with

Coomassie Blue; fractions containing myosin XIa were pooled together. The protein was then concentrated using a Millipore Stirred Ultrafiltration with 25 mm Millipore Ultrafiltration Membranes with a 10,000 MW cut off, and buffer exchanged into 10 mM sodium phosphate pH 7.4, 140 mM NaCl and 10% (v/v) glycerol buffer using a NAP 25 column (GE LifeSciences). A ninhydrin assay was then performed to determine protein concentration (Rosen, 1957). 100  $\mu$ L aliquots were frozen in liquid nitrogen and then stored at  $-80^{\circ}\text{C}$ .

### **2.2.2 Rab GTPases Wild Type and Mutants**

Proteins were expressed as described for myosin XIa above. After overnight growth, cells were harvested through centrifugation at  $4^{\circ}\text{C}$  at 5000 rpm (Sorvall Evolution centrifuge with a SLC-6000 rotor) for 10 minutes. The pellet from 250 mL of culture was resuspended in 15mL of lysis buffer (20 mM Tris pH8, 300 mM NaCl, 1 mM DTT). Then cells were lysed using a microfluizer cell disrupter at 80 psi. Lysed cells were centrifuged at 13000 rpm for 30 minutes at  $4^{\circ}\text{C}$  in a Sorvall SS-34 rotor. 50  $\mu$ L of magnetic glutathione resin (Pierce) was added to the supernatant and rocked on a nutator for 90 minutes. The beads were then centrifuged to the bottom of the tube and the supernatant removed. Beads were washed 3-4 times with 500  $\mu$ L buffer and separated into 3 tubes ( $\sim$ 100  $\mu$ L each) for nucleotide exchange. 10  $\mu$ L of each RabA was added to a fourth tube, the liquid was removed and the beads were boiled in 10  $\mu$ L 1x SDS dye for 5 minutes. 7.5  $\mu$ L was then run on a gel to determine the concentration based on a myosin XIa standard.

10  $\mu$ L of 0.1 M GDP (in  $\text{diH}_2\text{O}$ ) was added to one tube and 10  $\mu$ L of 0.1 M GTPimido (in  $\text{diH}_2\text{O}$ ), a non-hydrolysable isoform GTP, was added to the second. 5  $\mu$ L of binding buffer (10 mM  $\text{NaHPO}_4$  pH 8, 140 mM NaCl, 10% (v/v) glycerol, 1 mM DTT, 1 mM EDTA, 5 mM  $\text{MgCl}_2$ ) was added to the last tube to generate an apo or non-nucleotide loaded form. The tubes

were then nutated overnight and washed into binding buffer (see above) to a final volume of 100  $\mu\text{L}$ .

## **2.3 BINDING STUDIES**

### **2.3.1 Twelve Point Binding Curves**

After overnight nucleotide loading, pre-equilibrated GST-Rab bound magnetic resin was added into binding buffer (10 mM  $\text{NaHPO}_4$ , pH 8; 140 mM  $\text{NaCl}$ ; 10% glycerol; 1 mM DTT; 1 mM EDTA; 5 mM  $\text{MgCl}_2$ ) and aliquoted in 12 Eppendorf tubes such that each of the 12 tubes had the same concentration of GST-Rab. The amount of beads was also standardized by diluting more concentrated Rab purifications into buffer-washed empty beads. The liquid was then removed from each tube after magnetic separation (NEB, Catalog #: S1506S), leaving GST-Rab magnetic resin with no visible liquid. Myosin XIa was serially diluted using binding buffer from 32  $\mu\text{M}$  to 0.03  $\mu\text{M}$ , to obtain 12 different concentrations. 30  $\mu\text{L}$  of myosin XIa dilution were added to each of the tubes of GST-Rab magnetic resin and 30  $\mu\text{L}$  binding buffer was added for the 0  $\mu\text{M}$  point. Tubes were incubated on a nutator at 4°C for one hour. Beads were spun down in a table top centrifuge and all the liquid was removed. Beads were washed in 60  $\mu\text{L}$  of binding buffer zero to three times, depending on the experiment. All liquid was then removed and beads were resuspended in SDS loading dye (2% (w/v) SDS; 2 mM DTT; 4% (v/v) Glycerol; 0.04 M Tris-HCL pH=6.8; 0.004% (w/v) bromophenol blue) according to Table 2.

**Table 2: Concentration of myosin XIa and volumes added in 12 point binding studies**

[Myosin XIa] (μM)	63.4	31.7	15.9	7.93	3.96	1.98	0.99	0.5	0.25	0.12	0.06	0
1x Dye Added (μl)	600	400	200	100	75	50	35	20	12	12	12	12

After samples were boiled in dye, 7.5 μL from each tube was loaded on a 10% SDS page gel and run at 100 V through the stacking gel, and then 200 V through the resolving gel. Gels, were krypton stained (Pierce, Catalog #: 46630). Gels were imaged using a fluorescence reader (GE LifeSciences) for Alexa Fluor-532 and a PMT of 600. Results were quantified by densitometry of the bands to find the fluorescence  $\left(\frac{\text{intensity of band} - \text{background intensity}}{\text{area of band}}\right)$  and normalized to a myosin standard (1.4 μg). GraphPad PRISM was then used to fit a one site binding saturation curve to the data. The equation was constrained with the background equal to zero as well as setting the maximum iterations between 1000 and 5000.

### **2.3.2 12.5 nM Binding Study Methodology**

After overnight nucleotide loading, 12.5 nM of each Rab condition (GTP, GDP, apo) and GST were added to 4 tubes, and all liquid was removed from the tube. Rabs were diluted in additional empty beads washed into binding buffer (10 mM NaHPO<sub>4</sub>, pH 8; 140 mM NaCl; 10% (v/v) glycerol; 1 mM DTT; 1 mM EDTA; 5 mM MgCl<sub>2</sub>; 0.5% (v/v) NP40) to keep the number of beads in each tube consistent. Myosin XIa-CCT was diluted to final concentrations of 5 μM, 2.5 μM and 0.25 μM with final concentrations of buffer components equal to those of the binding buffer. Then 100 μL of each dilution of myosin XIa-CCT were added to each Rab

condition and GST alone, and allowed to nutate for 1 hour at 4°C. Beads were spun down in a tabletop centrifuge and all the liquid from each tube was removed. 24 µL of 1x SDS dye was added to the each tube and spun down. Samples were boiled for 7 minutes, and then spun again.

Gels were ran and analyzed as in the binding curve methodology but instead of dividing by a standard, a molar ratio of myosin to the RabA or GST was calculated using the densitometry values normalized by each protein's molecular weight. These molar ratios were compared using an ANOVA with multiple comparisons to determine statistical significance.

### **2.3.3 2.5 µM Binding Study**

Experiment was repeated as in 12.5 nM study, with 2.5 µM of each RabA protein and GST and only 5 µM myosin XIa. After one hour nutation, beads were washed in 100 µL of binding buffer three times. 50 µL of dye was added after each reaction was complete and each sample was run on a 10 % SDS-PAGE gel. A Western blot was performed by first transferring the proteins from the gel to a nitrocellulose membrane. 6 mL of PBS, 0.5% (v/v) Tween and 5% (w/v) milk was added to the nitrocellulose overnight to block the membrane. The next day, the membrane was incubated for one hour with a primary antibody, previously generated against the myosin XIa GTD, diluted in 6 mL final volume of PBS Tween at 1/500 final dilution. The membrane was washed three times in PBS Tween, three times in PBS and three times again in PBS tween, with the third incubating for 30 minutes. Next, a Goat anti-Rabbit secondary antibody diluted in PBS Tween at 1/1000 final dilution was added and nutated for 40 minutes. The wash protocol was repeated and then a 50:50 ratio of the Western blot detection reagents (Pierce, Catalog #: 21050) were added to the membrane for exactly 1 minute. The membrane was then imaged using a chemiluminescence imager (GE LifeSciences). Results were quantified as described in the binding curve protocol and analyzed for visual differences in the data.

## 3.0 RESULTS

---

### 3.1 SITE DIRECTED MUTAGENESIS

Both myosin XIa and RabA21 were mutagenized using the New England Biolabs Q5 Mutagenesis Kit as described in the Methodology section. The myosin XIa mutations were made based on the results of the RNAi complementation assay (**Figure 7**) for use in future binding studies. The RabA21 mutants were created based on mutants described in Ypt31/32p from *S. cerevisiae* (Lipatova et al., 2008). These mutants were predicted to lock RabA21 in conformations analogous to a nucleotide state for use in binding studies (S26N and N124I are predicted to be dominant negatives and Q71L is predicted to be constitutively active).

The PCR products obtained for each mutation were run on an agarose gel, shown below in

**Figure 9.**

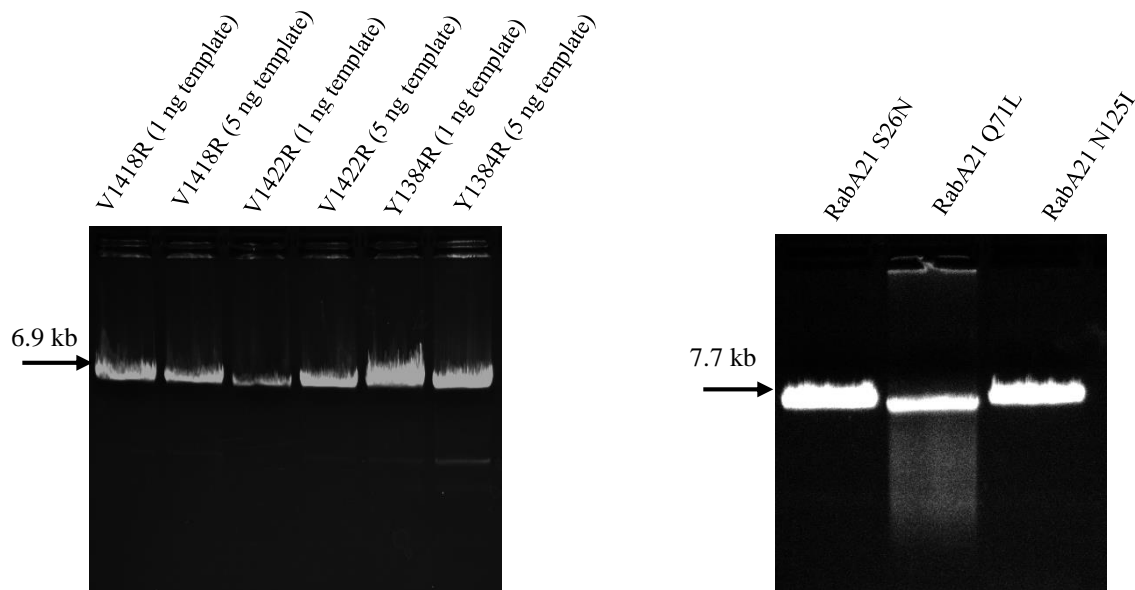


**Figure 9: PCR product from Q5 mutagenesis reactions for myosin XIa and RabA21**

As shown in the figure, a PCR product with the expected size of 6.9 kb for myosin XIa and 7.7 kb for Rab A21 was obtained for each mutant. After a gel purification step, each PCR product was used to transform *E. coli* and the presence of the mutation was confirmed in each plasmid via sequencing. The expression plasmids were then used to recombinantly express the *P. patens* proteins to be purified.

## **3.2 PROTEIN PURIFICATIONS**

### **3.2.1 Wild type and Mutant Myosin XIa-CCT Purification**

Plasmids containing each versions of the myosin XIa coiled-coil tail (CCT) construct (Wild type, Y1384, V1418R, V1422R) were transformed into BL21(DE3) *E. coli* competent cells and grown at 37°C to an OD<sub>600</sub> of approximately 0.6. IPTG was then added, and induction proceeded overnight at 15°C. Whole cell lysate was then purified through a nickel-NTA resin and then over an anion exchange column. Fractions were collected and run on a 12% SDS PAGE gel, as shown in **Figure 10**.

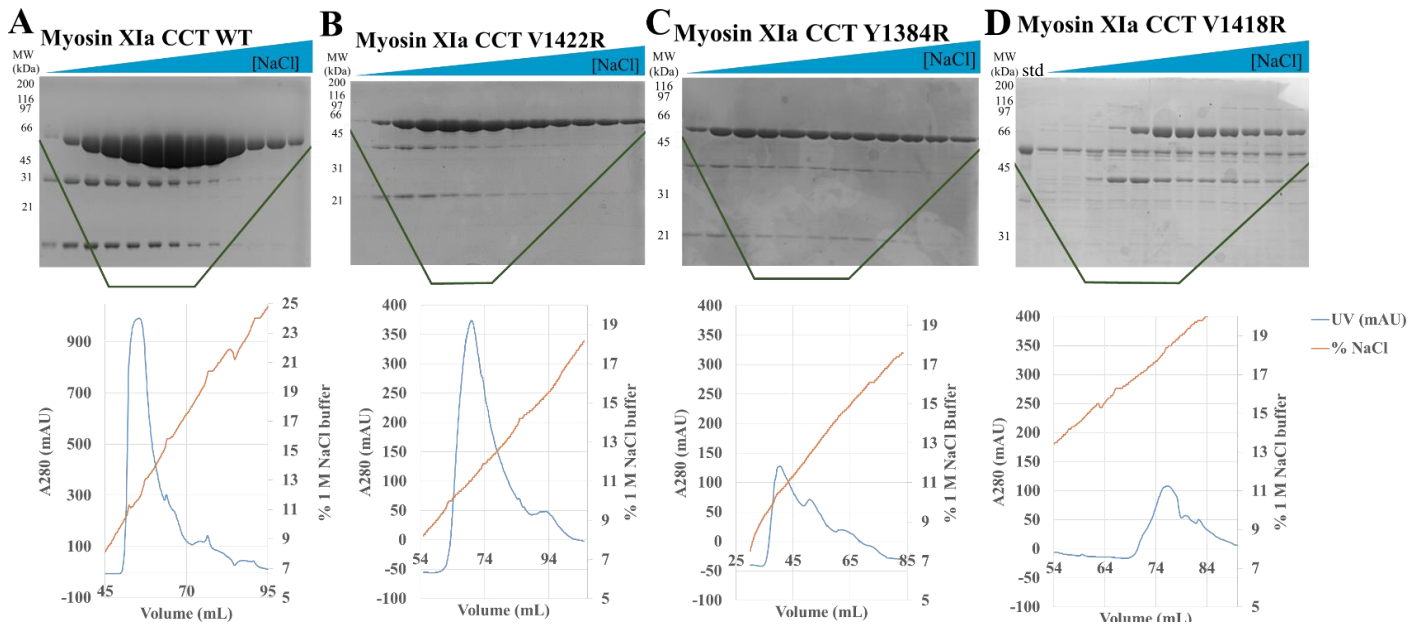


**Figure 10: Purification of myosin XIa (MW 58kDa)** Upper Panel: MonoQ fractions on SDS-PAGE gel; Lower Panel: Chromatographs A) Wild Type (10 L) B) V1422R (5 L) C) Y1384R (5 L) D) V1418R (10L), Purified Myosin XIa Std. in first lane

V1422R and Y1384 were able to be purified similarly to the wild type, with the wild type having a higher yield due to a 10 L culture of *E. coli* as compare to a 5 L culture for each mutant (**Figure 10, B and C**). However, the V1418R mutant protein was unable to be successfully purified and came off the MonoQ uniformly (**Figure D**). This is likely due to protein misfolding and forming insoluble aggregates both in the cell pellet during centrifugation and throughout the purification. This results is consistent with the Myo5B vs. myosin XIa modelling which predicted the residue to be internal.

The fractions containing each purified protein were then pooled and concentrated. A ninhydrin assay was then performed to find the concentration of each protein, the results of which are shown in **Figure 11**.

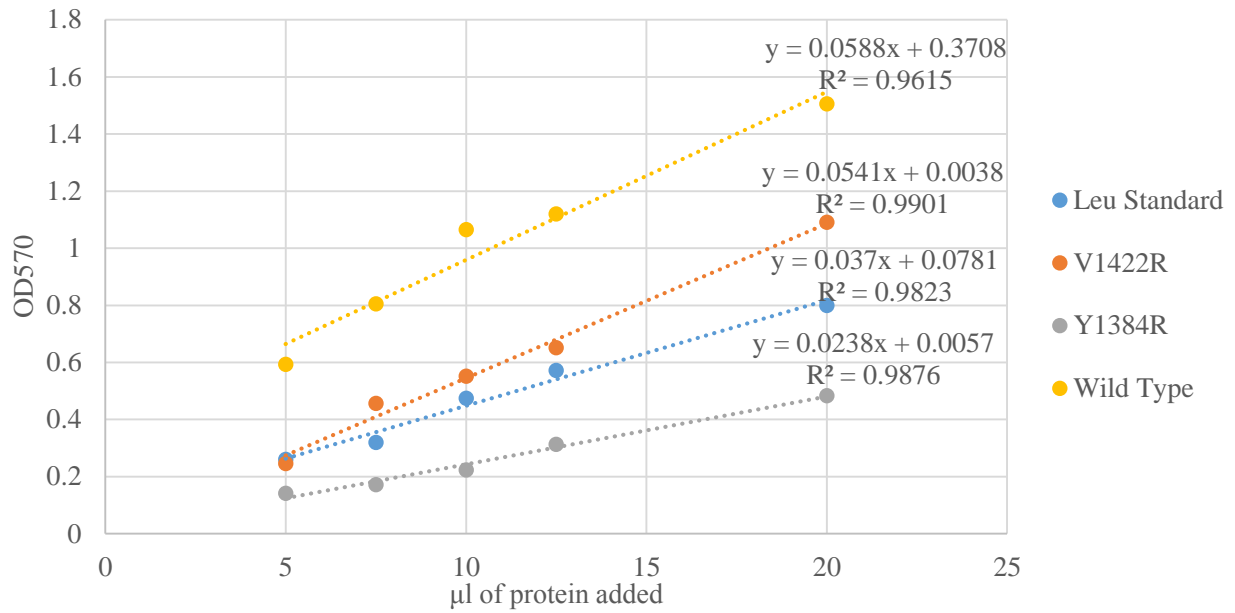


**Figure 11: Myosin XIa ninhydrin assay**

The concentrations were then calculated from the ratio of the leucine and myosin slopes in **Figure 11**. Wild type myosin was concentrated to 32 μM, V1422R was concentrated to 29.6 μM and Y1384R was concentrated to 12.99 μM. These three proteins were then flash frozen with liquid nitrogen in 100 μL aliquots and stored at -80°C for future binding studies.

### 3.2.2 RabA21, A41, and A53 WT and RabA21 Mutants Purification

GST, wild type RabAs and RabA21 mutants were transformed into BL21(DE3) *E.coli* and grown at 37°C to an OD<sub>600</sub> of approximately 0.6. IPTG was then added to induce the T7 promoter, and induction proceeded overnight at 15°C. The GST-Rabs were purified from whole cell lysate through a pull out with magnetic glutathione resin which were used in the binding studies. To quantify the concentration of RabA or GST, a sample was taken and the beads were boiled in dye and run on an SDS-PAGE gel (**Figure 12A**). Each RabA and GST migrated as expected on the gel to their respective sizes: RabA21 (51.6 KDa) RabA41 (52.3 KDa) RabA53 (51.3 KDa) GST (26.3 KDa). RabA21 mutants purified similarly to the wild type with a similar range of concentrations (**Figure 12B**).

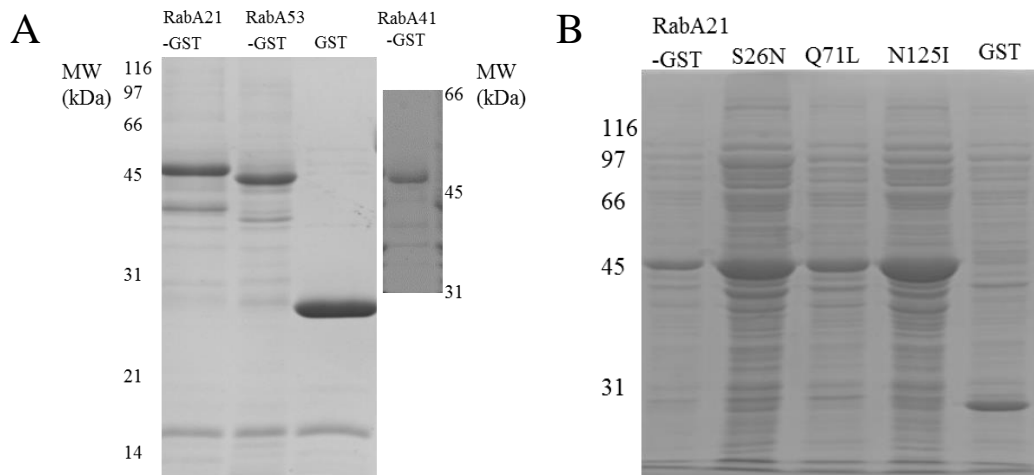


**Figure 12: RabA wild type and mutant purification** A) Representative gel of Wild type Rab and GST B) RabA21, RabA21 mutants and GST

Each RabA21 mutant had approximately the same molecular weight (51.5 kDa) and so ran to the same point in each lane. RabA and GST were freshly purified for each binding study, and concentrations ranged between 1-6  $\mu$ M when compared to a myosin XIa standard. The single step purification protocol, however, produced a somewhat impure sample as can be seen in the

many contaminant bands in **Figure 12**. Since the contaminants were consistent across the Rabs, the contaminants were accepted as background in all of the binding assays.

### 3.3 RABA-MYOSIN XIa-CCT BINDING STUDIES

Binding studies were performed to demonstrate a physical interaction between the purified myosin XIa-CCT and at least one of the RabA proteins which were purified. The three RabAs tested, RabA21, RabA41, RabA53, were chosen based on homology to the mammalian Rab11. Expected results included an increase in binding in the GTP-loaded form of the RabA, as seen by a lower  $K_d$  in binding curves or an increase in overall binding in the binding differentials experiments. These experiments allow for quantification of myosin XIa binding to Rab and could allow for the determination of the  $K_d$ .

#### 3.3.1 Binding Curve

A binding curve was created by performing a 12 point two-fold serial dilution of the wild type 32  $\mu\text{M}$  myosin XIa-CCT and adding each concentration to 0.3  $\mu\text{M}$  RabA-GST on glutathione resin. After one hour incubation, the liquid was removed, zero to three washes were performed (experiment dependent), and the remaining myosin was quantified on an SDS PAGE gel. Representative results for each of the three RabA proteins are shown in **Figure 13**.

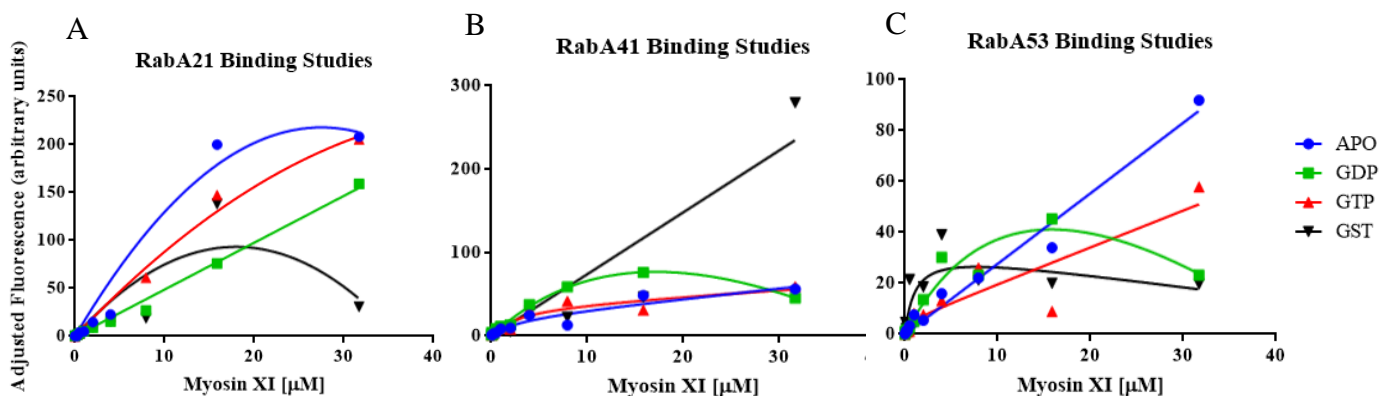


**Figure 13:** Twelve point binding curve experiments A) RabA21 B) RabA41 C) RabA53

A representative binding curve for each RabA is shown (**Figure 13**) in the GTP, GDP and APO nucleotide loaded state, along with a GST control. RabA21 and RabA53 had myosin XIa binding around or above the level of binding to the GST control, while RabA41 was below the control for most concentrations tested. The data, however, were highly inconsistent and noisy, as can be seen in the major differences between the GST curves in each panel of **Figure 13**. The variation in the data prevented the nonlinear regression software, GraphPad PRISM, from being able to accurately fit a binding curve to the data. These data suggest, however, that RabA21 and/ or RabA53 could be binding specifically to the myosin XIa-CCT, while RabA41 likely does not have any specific binding. An approximate  $K_d$  for each RabA was determined to be in the low  $\mu\text{M}$  range, but no further precision was possible. Optimization of the binding curves was needed for more conclusive results regarding a specific binding interaction between the myosin XIa and a RabA-GTP.

### **3.3.2 Binding Differential (12.5 nM)**

As an attempt to minimize the noisiness of the data shown in **Figure 13**, the concentration of RabA in each condition was decreased to 12.5 nM and no washes were performed. Additionally, instead of creating a binding curve using many protein concentrations, only three myosin XIa concentrations were used; a concentration near the approximate  $K_d$  (2.5  $\mu\text{M}$ ) and concentrations above and below this concentration (5 and 0.25  $\mu\text{M}$ ). While binding at the low and high concentrations of myosin XIa should show similar levels of myosin XIa binding to the RabA, points near the  $K_d$  should have greater differences in binding between the active and inactive state of the RabA and between the RabA proteins. Non-specific binding, however, should show no differences in binding between nucleotide state or Rab at a given concentration. The results from this binding experiment are shown in **Figure 14**.

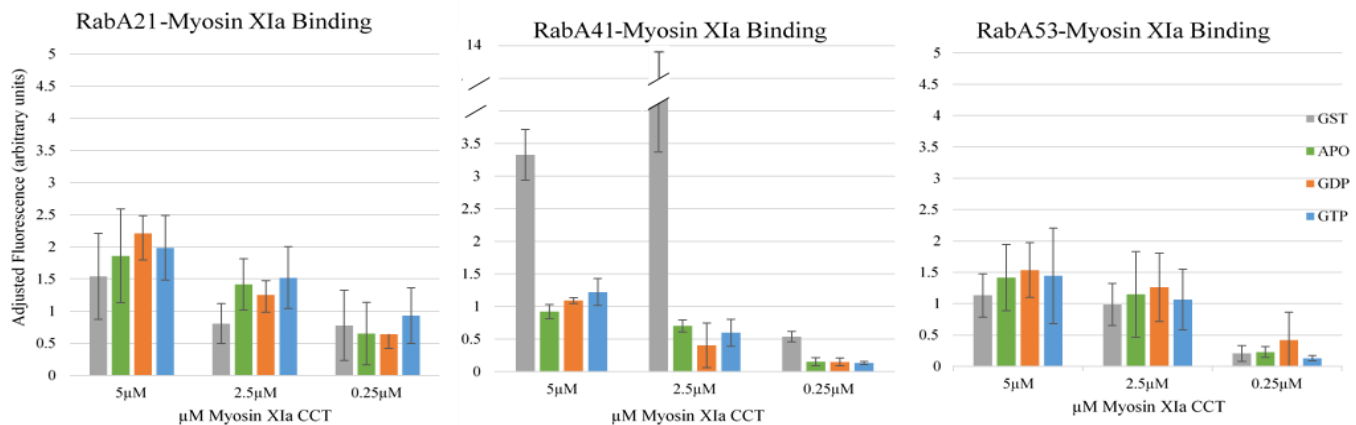


**Figure 14: Binding differentials experiment (12.5 nM) A) RabA21 (n=6) B) RabA41 (n=3) C) RabA53 (n=6)**

As seen in **Figure 14**, RabA41 bound to myosin XIa significantly below the binding to GST, but RabA21 and RabA53 bound at or slightly above the binding to the GST control. Additionally, no significant differences were seen between the different nucleotide states, as would be expected based on previous knowledge of class V myosin and Rab interactions (Pylypenko, 2013). While the concentration of RabA protein on the beads was decreased in an effort to minimize nonspecific binding, a possible cause of the variation in **Figure 13**, the specific signal was also greatly decreased in these experiments. Furthermore, at 12.5 nM RabA, any washing depleted the specific signal as well as nonspecific binding. Because specific signal was low due to the low concentration of Rab and nonspecific signal was high due to a lack of washes, the signal to noise ratio was too low to confidently draw conclusions from the data. Further work needed to be done to differentiate the binding between RabA21 and RabA53 and increase the signal to noise ratio.

### 3.3.3 Binding Differential (2.5 $\mu\text{M}$ )

To overcome a potentially large off-rate of this reaction, the RabA concentration was increased to 2.5  $\mu\text{M}$  and 5  $\mu\text{M}$  myosin XIa was used. This higher concentration was used to saturate the system, so that despite the potentially large off-rate of the reaction, there is enough RabA and myosin XIa to still have a percentage of the myosin XIa binding to the RabA. Having this saturation of the reaction allowed for the resin to be washed three times after nutation to minimize non-specific binding, but still have some of the specific binding remaining. The concentration of myosin XIa bound to the beads were then quantified by Western blot to be able clearly visualize the myosin XIa signal despite contaminants from the RabA purification (**Figure 15**).

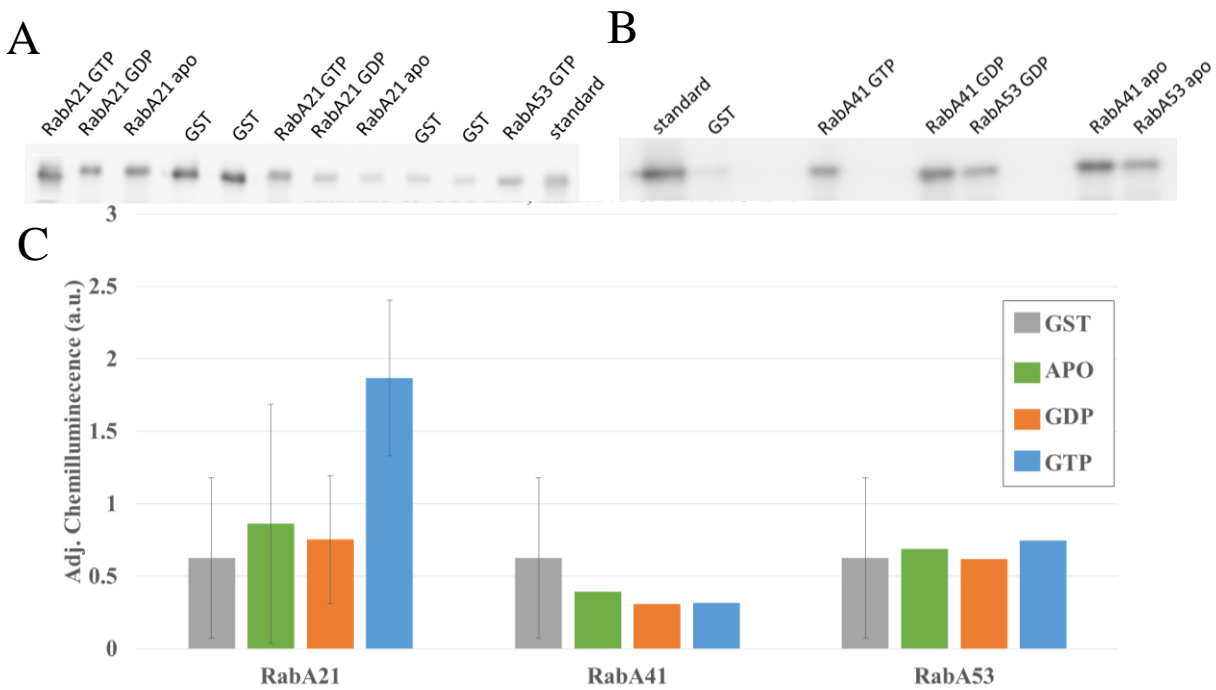


**Figure 15: Binding differentials experiment (2.5  $\mu\text{M}$ )** A) and B) display Western blots from RabA21 ( $n=2$ ), RabA41 ( $n=1$ ), RabA53 ( $n=1$ ) and GST ( $n=4$ ). Blots were performed using a myosin XIa antibody, which is quantified in C). Standard was 0.16  $\mu\text{M}$  purified Myosin XIa.

While RabA41 and RabA53 bound myosin XIa-CCT at or below the binding to the GST control, RabA21 GTP bound myosin XIa bound approximately three fold over the GST control and other nucleotide states. This data suggests that RabA21 GTP is binding to myosin XIa-CCT at a higher level than the other RabA proteins tested or the GDP state. However, the GST signal in these two trials greatly differed in intensity. Since only one (RabA41 and RabA53) or two (RabA21) replicates were performed, this experiment would need to be repeated to be confirmed.

### **3.3.4 RabA21 Nucleotide Locking**

Since the amount of successfully loaded nucleotide is unknown, RabA21 locked mutants were created and tested in the same protocol as the previous experiment. These mutants were modelled against the *S. cerevisiae* Ypt31/32p mutants to potentially induce a conformation change in Rab21 which is analogous to the nucleotide loaded states (S26N and N125I are predicted to be dominant negative and Q71L is predicted to be constitutively active). Therefore, the binding of Q71L-RabA21 should represent the binding if the GTP loading was perfectly efficient and be significantly above the GST control. The binding of S26N-RabA21 and N125I-RabA21 should represent the binding in the inactive state of the Rab, and should be equivalent to the control. The experimental Western blots and their quantification can be seen in **Figure 16**.

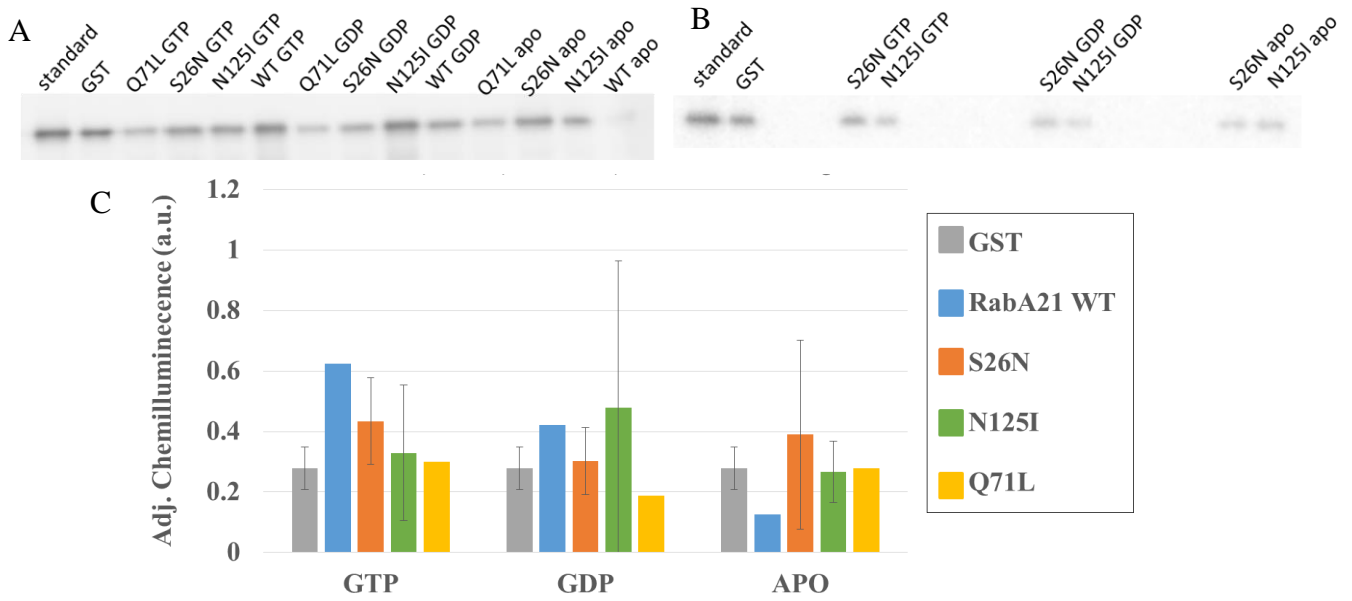


**Figure 16: Binding differentials (2.5  $\mu$ M) RabA21 mutants A) and B) trial one and two of the RabA21 mutant study C) quantification of western blot data. Standard was 0.16  $\mu$ M purified Myosin XIa.**

No conclusions about the nucleotide state required for RabA21 binding to myosin XIa can be drawn from **Figure 16**. WT-RabA21 GTP had a higher signal than any of the mutants, including the hypothesized constitutively active mutant (Q71L). There was also large variation when two trials were performed with the dominant negative mutants (N125I and S26N), which would be expected from non-specific binding. However, due to the fact that the constitutively active mutant (Q71L) had lower binding than the dominant negative mutants (S26N and N125I) and the wild type RabA, these mutations are likely not properly locking the RabA into the proper nucleotide loaded conformation. Due to the high concentration of RabA necessary and the yield limitations of the Rab purification protocol, the experiment was limited to only one (RabA21 WT and Q71L) or two (S26N and N125I) trials. Further work would be needed to characterize the true conformations of these mutants before they could be effectively used in future binding studies.

## 4.0 DISCUSSION

---

Polarized tip growth is an important process in many organisms. In *Physcomitrella patens*, myosin XIa trafficking along actin is necessary for polarized growth (Vidali et al., 2010). It is predicted that at least one RabA is necessary for recruitment of cargo to myosin XIa in *P. patens*, based on homology to the mammalian Rab11. In previous studies, mutations in myosin XIa proteins were determined to inhibit polarized growth through an RNAi complementation assay, and were predicted to disrupt myosin XIa RabA binding (Armstrong, 2012). This study investigated which RabA binds to myosin XIa and purified mutants from the RNAi complementation assay which could be disrupting the binding to a RabA.

The results from the modeling and myosin XIa-CCT purification suggest that V1422R is most likely to be an exposed surface residue, which could have a phenotype due to disruption of the myosin-Rab binding interface. On the other hand, V1418R is likely an internal hydrophobic residue based on the modeling, which renders it insoluble in the purification.

The described results indicate several conclusions regarding the interaction between myosin XIa and RabA21 in *Physcomitrella patens*. Firstly, the data in **Figure 15** indicates that RabA21 binds the globular tail domain of myosin XIa in its GTP-loaded form. This binding is in stark contrast to the interaction with RabA41, which does not physically associate with the myosin XIa-CCT in any of the binding assays performed.

At this junction in the project, however, more work remains to be done in optimizing the binding studies between myosin XIa and RabA. While the data regarding the myosin XIa-RabA21 interaction is promising, the data remains somewhat inconsistent and difficult to conclusively interpret. The variance in the data could be due to many reasons. Firstly, the

variation and relatively low binding affinity could be due to a mixed population of nucleotide state. If the current nucleotide exchange protocol does not efficiently strip the nucleotide in place at the time of purification and insert the desired nucleotide, this would result in mixed populations within a given experimental condition. This mixed population could then lead to only a small or varying percentage of RabA21 molecules being in an active binding conformation, causing both apparently weak or the experimentally observed variance in binding. A variety of spectroscopic or biophysical approaches could be employed to identify the bound nucleotide in each RabA for future studies.

Secondly, the binding studies could be optimized by attaching each of the RabAs to liposomes. Since Rab-GTPases are prenylated on their C-terminal domain, they efficiently embed into the membrane of cells (Mizuno-Yamasaki, 2012). Thus far, the recombinant RabAs have been GST-tagged on their N-terminus in an attempt to replicate the effect on the membrane. This method, however, likely poorly approximates the conformational changes associated with imbedding in the membrane, which could be inhibiting binding. By attaching each of the RabAs to liposomes and therefore introducing a bilayer membrane, the *in vivo* binding conditions may be more accurately replicated *in vitro*. Since RabAs are embedded in the membrane in their active form, the membrane may have a role in binding, such as PI4P's role in yeast (Mizuno-Yamasaki et al., 2010; Santiago-Tirado et al., 2011). This has been done previously for human Rabs to determine their role in membrane tethering as well as endosomal tethering in yeast (Lo, 2012; Tamura, 2014).

Thirdly, the relatively low affinity of the RabA to myosin XIa could be due to the absence of an adapter protein. Other Rab-myosin interactions are mediated by additional proteins, such as mammalian Rab11-FIP2 which is implicated in the recycling of endosomes and receptor-

mediated endocytosis and dRib11 which is important for rhodopsin transport (Cullis, 2002; Li, 2007). An analogous system could be at work in *P. patens* where a RabA-myosin XIa interaction is stabilized or guided by an unknown adapter protein not present in the *in vitro* binding studies. One potential test for such an adapter protein could include a binding study with the addition of *P. patens* lysate. While this method eliminates much of the potential quantification power of the experiment, a significant increase in binding with the addition of lysate would suggest that the lysate contained an adapter necessary for efficient binding.

Fourthly, the binding studies could be expanded to include many of the other RabAs present in *P. patens*. Thus far only three representative Rab-GTPases have been tested, but these may not be involved in physical interaction with myosin XIa. If the optimization steps previously described do not produce reproducible and significant results, the reason could be merely that the correct Rab binding partner has not yet been tested.

Finally, if binding studies prove to be an ineffective means of identifying a Rab-myosin interaction in *P. patens*, other assays could be used to identify a physical interaction. Namely, mass spectrometry could be used to identify the proteins which bind to the CCT portion of myosin XIa. In this experiment, purified myosin XIa-CCT would be covalently attached to beads. *P. patens* cell lysate would then be incubated with the beads to allow binding to occur. After washing, all the proteins bound to the myosin XIa-CCT would be analyzed via mass spectrometry. Unlike the binding studies, this method allows for all the proteins in moss lysate to be analyzed at once for potential binding partners. Another potential experiment could utilize a yeast two hybrid screen using the myosin XIa cargo binding domain as bait. This strategy was successfully employed in *Arabidopsis thaliana* to identify the myosin XIa receptor, but is also prone to both false positives and negatives (Peremyslov, 2013).

Once a myosin XIa-RabA interaction is confirmed, the myosin XIa mutants should be analyzed in the same method as the wild type myosin XIa. If a defect in binding is observed with a mutant, this would support the hypothesis that the growth defect observed in the RNAi complementation assay for that mutant was due to an inhibition of binding with the Rab-GTPase. In the binding assay, this would manifest as an increase in the  $K_d$  and a decrease in overall binding. In the mass spectrometry assay, this would be seen by the RabA no longer being pulled down by the myosin XIa or being pulled down in decreasing quantities. Ultimately, the *P. patens* myosin XIa-RabA interaction would be best characterized by solving the crystal structure of the proteins in complex with one another. This would clearly identify the binding interface on both binding partners and confirm the physical interaction between them. These types of experiments were employed successfully by the Weismann lab in the *S. cerevisiae* system with Myo2p and Ypt31/32p (Pashkova et al., 2006; Lipatova et al., 2008).

Thus far, this research has demonstrated the promise in utilizing the tip cells of *Physcomitrella patens* to study the participation of myosin XIa in the complex processes of polarized growth. While more work needs to be done, RabA21-GTP has been identified as a viable candidate for a Rab-myosin interaction necessary for polarized growth.

## 6.0 REFERENCES

---

- Agar, E.** (2013). Interactions between myosin XIa and rab proteins in the moss *Physcomitrella patens*. In Major Qualifying Project, W.P. Institute, ed.
- Armstrong, E.** (2012). Characterization of the Interaction Between Myosin XIa and RabA4 in *Physcomitrella patens*. In Major Qualifying Project, W.P. Institute, ed.
- Barr, F.** (2012). Rab GTPase and membrane identity: casual or inconsequential. *J. Cell Biol.* **202**, 191-199.
- Bernardo J. Foth, M.C.G., and Dominique Soldati.** (2006). New insights into myosin evolution and classification. *PNAS* **103**, 3681-3686.
- Callahan, K.** (2014). Analysis of Myosin XI and RabA Relationships during Polarized Tip Growth in *Physcomitrella patens*. In Major Qualifying Project, W.P. Institute, ed.
- Ciencia, I.G.d.** (2011). RabDB (Computational Genomics Laboratory).
- Cole, R.A., and Fowler, J.E.** (2006). Polarized growth: maintaining focus on the tip. *Current Opinion in Plant Biology* **9**, 579-588.
- Cove, D.J., and Knight, C.D.** (1993). The Moss *Physcomitrella patens*, a Model System with Potential for the Study of Plant Reproduction. *Plant Cell* **5**, 1483-1488.
- Cullis, D.N.P., Betsey; Baleja, James; Feig, Larry.** (2002). Rab11-FIP2, an Adaptor Protein Connecting Cellular Components Involved in Internalization and Recycling of Epidermal Growth Factor Receptors. *JBC* **277**, 49158-49166.
- Furt, F., Liu, Y.C., Bibeau, J.P., Tüzel, E., and Vidali, L.** (2013). Apical myosin XI anticipates F-actin during polarized growth of *Physcomitrella patens* cells. *Plant J* **73**, 417-428.
- Geeves, M.A., Holmes, K.C. .** (2005). The molecular mechanism of muscle contraction. *Adv. Protein Chem* **71**, 161-193.
- Goodsell, D.** (2001). Myosin. Molecule of the Month: Protein Data Bank.
- Jacques, M.** (2013). Purification of Myosin XI and Sec15 from *Physcomitrella patens*. In Major Qualifying Project, W.P. Institute, ed.
- Kamisugi, Y., Schlink, K., Rensing, S.A., Schween, G., von Stackelberg, M., Cuming, A.C., Reski, R., and Cove, D.J.** (2006). The mechanism of gene targeting in *Physcomitrella patens*: homologous recombination, concatenation and multiple integration. *Nucleic Acids Res* **34**, 6205-6214.

- Li, B.X.S., A.K.; Ready, D.F. .** (2007). Myosin V, Rab11, and dRip11 direct apical secretion and cellular morphogenesis in developing *Drosophila* photoreceptors. *J Cell Biol* **177**, 659-669.
- Lipatova, Z., Tokarev, A.A., Jin, Y., Mulholland, J., Weisman, L.S., and Segev, N.** (2008). Direct Interaction between a Myosin V Motor and the Rab GTPases Ypt31/32 Is Required for Polarized Secretion. *Molecular Biology of the Cell* **19**, 4177-4187.
- Lo, S.Y., Brett, C.L., Plemel, R.L., Vignali, M., Fields, S., Gonen, T. and Merz, A. J.** (2012). Intrinsic tethering activity of endosomal Rab proteins. *Natural Structural & Molecular Biology* **19**, 40-47.
- Maravillas-Montero J., S.-A., L.** (2012). The myosin family: unconventional role of actin-dependent molecular motors in immune cells. *J. of Leukocyte Bio* **91**, 35-46.
- Menand, B., Calder, G., and Dolan, L.** (2007). Both chloronemal and caulonemal cells expand by tip growth in the moss *Physcomitrella patens*. *J Exp Bot* **58**, 1843-1849.
- Mizuno-Yamasaki, E., Medkova, M., Coleman, J., and Novick, P.** (2010). Phosphatidylinositol 4-phosphate controls both membrane recruitment and a regulatory switch of the Rab GEF Sec2p. *Dev Cell* **18**, 828-840.
- Mizuno-Yamasaki, E., Felix Rivera-Molina, and Peter Novick.** (2012). GTPase networks in membrane traffic. *Annual review of biochemistry* **81**, 637.
- Pashkova, N., Catlett, N.L., Novak, J.L., and Weisman, L.S.** (2005). A point mutation in the cargo-binding domain of myosin V affects its interaction with multiple cargoes. *Eukaryotic Cell* **4**, 787-798.
- Pashkova, N., Jin, Y., Ramaswamy, S., and Weisman, L.S.** (2006). Structural basis for myosin V discrimination between distinct cargoes. *Embo Journal* **25**, 693-700.
- Peremyslov, V.V.M., E.A.; Kurth, E.G.; Makarova, K.S.; Koonin, E.V.; Dolja, V.V.** (2013). Identification of myosin XI receptors in *Arabidopsis* defines a distinct class of transport vesicles. *Plant Cell* **25**, 3022-3038.
- Pollard T.D., C.J.A.** (2009). Actin, a Central Player in Cell Shape and Movement *Science* **326**, 1208-1212.
- Pruyne D., B.A.** (2000). Polarization of cell growth in yeast. I. Establishment and maintenance of polarity states. *J Cell Sci* **113**, 365-375.
- Pylypenko, O.A., W.; Gauquelin, C.; Lahmani, M.; Coulibaly, D.; Baron, B.; Hoos, S.; Titus, M.A.; England, P.; Houdusse, A.M.** (2013). Structural basis of myosin V Rab GTPase-dependent cargo recognition. *PNAS* **110**, 20443-20448.
- Rensing, S.A., Lang, D., Zimmer, A.D., Terry, A., Salamov, A., Shapiro, H., Nishiyama, T., Perroud, P.F., Lindquist, E.A., Kamisugi, Y., Tanahashi, T., Sakakibara, K., Fujita,**

- T., Oishi, K., Shin, I.T., Kuroki, Y., Toyoda, A., Suzuki, Y., Hashimoto, S., Yamaguchi, K., Sugano, S., Kohara, Y., Fujiyama, A., Anterola, A., Aoki, S., Ashton, N., Barbazuk, W.B., Barker, E., Bennetzen, J.L., Blankenship, R., Cho, S.H., Dutcher, S.K., Estelle, M., Fawcett, J.A., Gundlach, H., Hanada, K., Heyl, A., Hicks, K.A., Hughes, J., Lohr, M., Mayer, K., Melkozernov, A., Murata, T., Nelson, D.R., Pils, B., Prigge, M., Reiss, B., Renner, T., Rombauts, S., Rushton, P.J., Sanderfoot, A., Schween, G., Shiu, S.H., Stueber, K., Theodoulou, F.L., Tu, H., Van de Peer, Y., Verrier, P.J., Waters, E., Wood, A., Yang, L., Cove, D., Cuming, A.C., Hasebe, M., Lucas, S., Mishler, B.D., Reski, R., Grigoriev, I.V., Quatrano, R.S., and Boore, J.L.** (2008). The *Physcomitrella* genome reveals evolutionary insights into the conquest of land by plants. *Science* **319**, 64-69.
- Rosen, H.** (1957). A modified ninhydrin colorimetric analysis for amino acids. *Archives of Biochemistry and Biophysics* **67**, 10-15.
- Santiago-Tirado, F.H., Legesse-Miller, A., Schott, D., and Bretscher, A.** (2011). PI4P and Rab inputs collaborate in myosin-V-dependent transport of secretory compartments in yeast. *Developmental Cell* **20**, 47-59.
- Scholey J. M., B.-M.I., Mogilner A. .** (2003). Cell Division. *Nature* **422**, 746-752.
- Tamura, N., Mima, J. .** (2014). Membrane-anchored human Rab GTPases directly mediate membrane tethering in vitro. *Biol Open* **3**, 1108-1115.
- Vale, R.D.** (2003). The molecular motor toolbox for intracellular transport. *Cell* **112**, 467-480.
- Vidali, L., and Hepler, P.K.** (2001). Actin and pollen tube growth. *Protoplasma* **215**, 64-76.
- Vidali, L., and Bezanilla, M.** (2012). *Physcomitrella patens*: a model for tip cell growth and differentiation. *Curr Opin Plant Biol* **15**, 625-631.
- Vidali, L., Burkart, G.M., Augustine, R.C., Kerdavid, E., Tüzel, E., and Bezanilla, M.** (2010). Myosin XI is essential for tip growth in *Physcomitrella patens*. *Plant Cell* **22**, 1868-1882.
- Wickner, W.T.S., R.** (2008). Membrane fusion. *Natural Structural & Molecular Biology* **15**, 658-664.
- Yumura S., U.T.Q.** (2003). Myosins and cell dynamics in cellular slime molds. *Int. Rev. Cytol.* **224**, 173-225.